J|A|C|S
ARTICLES
Published on Web 12/28/2007

Intermolecular Interaction-Induced Hierarchical Transformation in 1D Nanohybrids: Analysis of Conformational Changes by 2D Correlation Spectroscopy

Ho Seok Park,[†] Yeong Suk Choi,[‡] Young Mee Jung,[§] and Won Hi Hong*[,†]

Department of Chemical and Biomolecular Engineering (BK21 Program), KAIST, Guseong-dong 373-1, Yusong-gu, Daejeon, Republic of Korea, Energy and Environment Laboratory, Samsung Advanced Institute of Technology (SAIT), P.O. Box 111, Suwon, Republic of Korea, Department of Chemistry, Kangwon National University, Chunchon 200-701, Republic of Korea

Received May 2, 2007; E-mail: whhong@kaist.ac.kr.

Abstract: We have examined both self-assembly and confinement effect in room-temperature ionic liquid (RTIL)-aluminum hydroxide hybrids (RAHs) to attain a fundamental understanding of special phenomena in nanoscale spaces as well as to design functional nanomaterials for practical applications. Phase-controlled one-dimensional (1D) RAHs were synthesized through a simple ionothermal process. The RAHs were hierarchically transformed in terms of the molecular structures, morphologies, and phases of the materials during the ionothermal process with respect to the concentration of RTIL. In addition to the hierarchical transformation, the RTIL/aluminum hydroxide nanohybrids revealed unexpected physical behaviors, including thermal transition variation of the RTIL in confined environments and a phase transition from nanosolid to nanoliquid affected by changes of the melting points. More importantly, intermolecular interaction induced-self-assembly and confinement effect of RTILs inside an integrated hybrid system, which have not been clearly explained to date, were analyzed by 2D infrared correlation spectroscopy (2D IR COS); dynamic behaviors of RTILs, i.e., sequentially spatial reorientation and kinetically conformational changes, were attributed to the interactions between RTILs and aluminum hydroxides. 2D IR COS offers a new way to interpret highly complex, veiled systems such as the formation mechanism of nanoparticles, biomineralization, self/supramolecular assembly, and nanoconfinement.

Introduction

Room-temperature ionic liquids (RTILs) have attracted considerable attention as functional materials applicable for solvents,[1a] catalysis,[1b] electrochemistry,[1c] separation,[1d, e] due to their unique and tunable properties. Recently, RTILs were used as templates or cosolvents in ionothermal synthesis, a new synthetic method based on solution chemistry, for fabricating RTIL/inorganic hybrid or inorganic nanomaterials.[2−4] Ionothermal synthesis, having advantages over conventional solution syntheses in terms of eliminating the complications associated with high hydrothermal pressures in a sealed autoclave and avoiding the post-addition of organic solvents, strongly depends on the ionic characteristic of RTILs.[2] Therefore, a combination of anions or interactive components with the cations of RTILs would yield a new class of nanostructured hybrids, RTIL/inorganic nanohybrids, resulting from preferential growth of building blocks via a self-assembly process.[4] Kinetic control during the formation of nucleating seeds with specific crystal phases also plays a crucial role in constructing the nanoshapes of these hybrids.[5]

One-pot assembled RTIL/inorganic nanohybrids are novel materials that can overcome intrinsic limitations attributed to fluidicity and low viscosity of pristine RTILs in terms of application to electrochemical devices. Furthermore, spatially confined-RTILs in RTIL/inorganic nanohybrids had appealing properties such as excellent catalytic activities, good ionic conductivities, high heat resistances, and melting point depression.[6] Unexpected physical behaviors, including glass transition variation of RTILs in confined environments and phase transition from nanosolids to nanoliquids affected by changes to the melting points,[7] are of prime importance from both scientific and applicative points of view.

[†] KAIST.
[‡] SAIT.
[§] Kangwon National University.

(1) (a) Welton, T. *Chem. Rev.* **1999**, *99*, 2071−2083. (b) Dupont, J.; de Souza, R. F.; Suarez, P. A. Z. *Chem. Rev.* **2002**, *102*, 3667−3692. (c) Buzzeo, M. C.; Evans, R. G.; Compton R. G. *ChemPhysChem* **2004**, *5*, 1107−1120. (d) Blanchard, L. A.; Hancu, D.; Beckman, E. J.; Brennecke, J. F. *Nature* **1999**, *399*, 28−29. (e) Fei, Z.; Geldbach, T. J.; Zhao, D.; Dyson, P. J. *Chem.−Eur. J.* **2006**, *12*, 2122−2130.
(2) (a) Cooper, E. R.; Andrews, C. D.; Wheatley, P. S.; Webb, P. B.; Wormald, P.; Morris, R. E. *Nature* **2004**, *430*, 1012−1016. (b) Parnham, E. R.; Wheatley, P. S.; Morris, R. E. *Chem. Commun.* **2006**, 380−382. (c) Parnham, E. R.; Morris, R. E. *J. Am. Chem. Soc.* **2006**, *128*, 2204−2205. (d) Ding, K.; Miao, Z.; Liu, Z.; Zhang, Z.; Han, B.; An, G.; Miao, S.; Xie, Y. *J. Am. Chem. Soc.* **2007**, *129*, 6362−6363. (e) Taubert, A.; Lia, Z. *Dalton Trans.* **2007**, 723−727.
(3) Park, H. S.; Yang, S. H.; Jun, Y. S.; Hong, W. H.; Kang, J. K. *Chem. Mater.* **2007**, *19*, 535−542.
(4) Park, H. S.; Choi, Y. S.; Kim, Y. J.; Hong, W. H.; Song, H. *Adv. Funct. Mater.* **2007**, 10.1002/adfm.200600935.
(5) (a) Jun, Y.; Choi, J.; Cheon, J. *Angew. Chem., Int. Ed.* **2006**, *45*, 3414−3439. (b) Jun, Y.; Lee, J. H.; Choi, J.; Cheon, J. *J. Phys. Chem. B* **2005**, *109*, 14795−14806.

Intermolecular interaction-induced self-assembly and confinement effect are important phenomena in nanoscience and nanotechnology. Self-assembly is a facile and significant bottom-up approach toward forming emerging superstructures of matters and controlling their shapes and sizes.[8] Nanoconfinement meanwhile promotes special quantum effects such as changes in the miscibilities, phase behaviors, and physicochemical properties of fluids confined within/interacting with solids.[9] Fundamental understanding of the morphological evolution of nanohybrids and confinement effect of RTILs in nanopores, however, has thus far proved elusive,[4,6] primarily due to the complexity of these systems and difficulties in monitoring kinetically conformational changes and spatial reorientation.

The main objective of this work is to clarify the intermolecular interaction-induced phenomena, such as the morphological evolution of RTIL/inorganic nanohybrids and the variation of phase behavior due to confinement effect, to design and fabricate functional nanomaterials as well as to elucidate physical phenomena in nanoscale spaces. The basic strategies used in this work are (1) fixing reaction conditions by selecting a representative RTIL and an inorganic precursor to remove ambiguity arising from changes in the reaction environments, (2) varying the ratio of RTIL and inorganic precursors to monitor morphological evolution dependent on component concentrations, and (3) analyzing data obtained from 2-dimensional infrared correlation spectroscopy (2D IR COS). 2D IR COS is a well-established analytical technique that provides considerable utility and benefit in various spectroscopic studies of complex systems. Some of the notable features of generalized 2D correlation spectra are: simplification of complex spectra consisting of many overlapped peaks; enhancement of spectral resolution by spreading peaks along the second dimension; establishment of unambiguous assignments through correlation of bands of selectively coupled by various interaction mechanisms; and determination of the sequence of spectral peak emergence.[10]

In the work, we report on the phase-controlled synthesis of one-dimensional (1D) RTIL-aluminum hydroxide hybrids (RAHs), depending on the concentration of 1-butyl-3-methylimidazolium tetrafluoroborate ([BMim][BF_4]) during a simple ionothermal process. The RTIL, [BMim][BF_4], is regarded as (i) a template and cosolvent agents to drive the formation of 1D shapes of nanohybrids and (ii) fluids confined within porous networks of an integrated hybrid system. Herein, we analyze self-assembly and confinement effect of 1D nanohybrids induced by intermolecular interactions between RTILs and aluminum hydroxide crystallites by employing a 2D correlation analysis.

Table 1. Chemical Composition, Content of Chemisorbed Water, Crystalline Phase of Aluminum Hydroxide, and Morphology of RAH 1, RAH 2, RAH 3, RAH 4, and RAH 5

	molar ratio ([BMim][BF_4]: Al(OC_4H_9)$_3$)	wt % of [BMim][BF_4][a]	wt % of chemisorbed water[b]	crystalline phase of aluminum hydroxide (AlOOH)	shape
RAH 1	2:1	76.25	9.06	hexagonal	rod
RAH 2	1:1	65.76	10.74	hexagonal	rod
RAH 3	1:2	44.73	22.92	orthorhombic (major)	rod + fiber (major)
RAH 4	1:3	30.49	24.27	orthorhombic	fiber
RAH 5	1:6	26.56	22.26	orthorhombic	fiber

[a] Weight % of [BMim][BF_4] was calculated by elemental analysis. [b] Weight % of chemisorbed water was determined by weight loss up to 400 °C of TGA curve.

Table 2. Thermal and Textural Properties of [BMim][BF_4], RAH 1, RAH 2, RAH 3, RAH 4, and RAH 5

	T_g (°C)	T_m (°C)	pore size (nm)[a]	surface area (m^2/g)[b]	pore volume (cm^3/g)
[BMim][BF_4]	−80.2	−76.3	-	-	-
conventional mixture	−86.9	−83.9	11.1	118	0.27
RAH 1	4.4	63.5	18.4	109	0.68
RAH 2	18.7	60.3	12.3	100	0.23
RAH 3	-	58.6	11.3	204	1.07
RAH 4	-	-	11.3	224	1.19
RAH 5	-	-	7.3	347	1.29

[a] Pore size was calculated by Barret−Joyner−Hallender (BJH) model. [b] Surface area was calculated by Brunauer−Emmett−Teller (BET) equation.

Experimental Section

Synthesis of RTIL/Aluminum Hydroxide Hybrids. Aluminum tri-sec-butoxide (1.309 g, Aldrich, 99.9%) was mixed with 1-propanol (3 mL, Aldrich), deionized water (0.309 mL), and 1-butyl-3-methylimidazolium tetrafluoroborate (0.33, 0.66, 0.99, 1.98, and 3.96 g, [BMim][BF_4] from C-TRI, 99.9%), respectively. The molar ratio of [BMim][BF_4] and aluminum tri-sec-butoxide was 2:1, 1:1, 1:2, 1:3, and 1:6. Two milliliters of 0.01 M HCl was added dropwise to the mixture. HCl was used as an acid catalyst, because self-assembly via a hydrogen bonding-co-$\pi-\pi$ stacking mechanism occurs under acidic conditions.[4] After mixing all chemicals at the controlled molar ratio, the pHs of the mixtures were adjusted between 5.96 and 6.18. The resulting mixtures were stirred at 60 °C for 120 min, followed by aging at 60 °C for 1 day. To complete gelation during ionothermal synthesis, the mixtures were heated to 120 °C for 2 days under ambient pressure. The obtained [BMim][BF_4]/aluminum hydroxide hybrids are notated as RAH 1−5 according to the molar ratio of [BMim][BF_4] and aluminum precursors from 2:1 to 1:6, respectively.

We calculated the margin of error by measuring values of the same samples three times in Table 1 and 2. Every result was averaged in the error range of ±1%.

(6) (a) Goettmann, F.; Sanchez, C. *J. Mater. Chem.* **2007**, *17*, 24−30. (b) Néouze, M. A.; Bideau, J. L.; Gaveau, P.; Bellayer, S.; Vioux, A. *Chem. Mater.* **2006**, *18*, 3931−3936. (c) Lunstroot, K.; Driesen, K.; Nockemann, P.; Gorller-Walrand, C.; Binnemans, K.; Bellayer, S.; Le Bideau, J.; Vioux, A. *Chem. Mater.* **2006**, *18*, 5711−5715. (d) Néouze, M. A.; Bideau, J. L.; Leroux, F.; Vioux, A. *Chem. Commun.* **2005**, 1082−1084. (e) Liu, Y.; Wang, M.; Li, J.; Li, Z.; He, P.; Liu, H.; Li, J. *Chem. Commun.* **2005**, 1778−1780. (f) Shi, F.; Zhang, Q.; Li, D.; Deng, Y. *Chem.−Eur. J.* **2005**, *11*, 5279−5288.

(7) (a) Bourlinos, A. B.; Herrera, R.; Chalkias, N.; Jiang, D. D.; Jhang, Q.; Archer, L. A.; Giannelis, E. P. *Adv. Mater.* **2005**, *17*, 234−237. (b) Bourlinos, A. B.; Chowdhury, S. R.; Jiang, D. D.; An, Y.-U.; Zhang, Q.; Archer, L. A.; Giannelis, E. P. *Small* **2005**, *1*, 80−82. (c) Bourlinos, A. B.; Chowdhury, S. R.; Herrera, R.; Jiang, D. D.; Zhang, Q.; Archer, L. A.; Giannelis, E. P. *Adv. Funct. Mater.* **2005**, *15*, 1285−1290.

(8) (a) Boal, A. K.; Ilhan, F.; DeRouchey, J. E.; Thurn-Albrecht, T.; Russell, T. P.; Rotello, V. M. *Nature* **2000**, *404*, 746−748. (b) Frankamp, B. L.; Boal, A. K.; Rotello, V. M. *J. Am. Chem. Soc.* **2002**, *124*, 15146−15147. (c) Storhoff, J. J.; Lazarides, A. A.; Mucic, R. C.; Mirkin, C. A.; Letsinger, R. L.; Schatz, G. C. *J. Am. Chem. Soc.* **2000**, *122*, 4640−4650. (d) Liu, J.; Mendoza, S.; Roman, E.; Lynn, M. J.; Xu, R.; Kaifer, A. E. *J. Am. Chem. Soc.* **1999**, *121*, 4304−4305. (e) Naka, K.; Itoh, H.; Chujo, Y. *Langmuir* **2003**, *19*, 5496−5501. (f) Caruso, F.; Caruso, R.; Möhwald, H. *Science* **1998**, *282*, 1111−1114.

(9) (a) Zhu, S.; Liu, Y.; Rafailovich, M. H.; Sokolov, J.; Gersappe, D.; Winesett, D. A.; Ade, H. *Nature* **1999**, *400*, 49−51. (b) Koga, K.; Gao, G. T.; Tanaka, H.; Zeng, X. C. *Nature* **2001**, *412*, 802−805. (c) Huck, W. T. S. *Chem. Commun.* **2005**, 4143−4148 (d) Hummer, G.; Rasaiah, J. C.; Noworyta, J. P. *Nature* **2001**, *414*, 188−190. (e) Zhu, L.; Cheng, S. Z. D.; Huang, P.; Ge, Q.; Quirk, R. P.; Thomas, E. L.; Lotz, B.; Hsiao, B. S.; Yeh, F.; Liu, L. *Adv. Mater.* **2002**, *14*, 31−34.

(10) (a) Ozaki, Y.; Noda, I. *Two-Dimensional Correlation Spectroscopy: Applications in Vibrational Spectroscopy*; John Wiley & Sons, Inc.: New York, 2004. (b) Jung, Y. M.; Noda, I. *Appl. Spectrosc. Rev.* **2006**, *41*, 515−547. (c) Noda, I. *Appl. Spectrosc.* **1993**, *47*, 1329−1336.

Characterization. SEM images were obtained by a Field Emission Scanning Electron Microscope (Philips SEM 535M), equipped with a Schottky based field emission gun.

TEM images were collected on an E.M. 912 Ω Energy-Filtering Transmission Electron Microscope (EF TEM, 120 kV) and a JEM-3010 High-Resolution Transmission Electron Microscope (HR TEM, 300 kV).

X-ray diffraction (XRD) data were obtained on a Rigaku D/max lllC (3 kW) with a θ/θ goniometer equipped with a Cu Kα radiation generator. The diffraction angle of the diffractograms was in the range of $2\theta = 10-80°$.

^{27}Al nuclear magnetic resonance (NMR) spectra were obtained by using a Bruker DSX 400 solid-state NMR spectrometer (400 MHz), equipped with a CP/MAS probe.

Thermogravimetric analyses (TGA) were performed using a Dupont 2200 thermal analysis station. Every sample was heated from 30 to 900 °C at a rate of 10 °C/min under a nitrogen atmosphere.

For BET measurements, [BMim][BF_4] was removed by solvent extraction with acetonitrile. The complete removal of C_4BF_4 was confirmed by evaluating the content of carbon and nitrogen of the isolated aluminum hydroxides by means of element analysis. N_2 sorption/desorption data were obtained using a gas sorption analyzer (NOVA 4200 Ver. 7.10). The specific surface areas were calculated by the BET equation, and pore sizes were determined by using the BJH model.

FT-IR ATR spectra were collected on a JASCO FT-IR 470 plus as attenuated total reflection. Each spectrum, which was recorded as the average of 12 scans with a resolution of 4 cm^{-1}, was collected from 4000 to 650 cm^{-1}.

Synchronous and asynchronous 2D correlation spectra were obtained using the same software as those described previously.[11] In light of recent publications concerning the normalization procedure in 2D correlation analysis,[11] we tested various methods and found that the best results were obtained using non-normalized data.

UV−vis spectra (190−600 nm) were recorded with the CE instrument after the samples were passed to contact the detector.

Differential scanning calorimetry (DSC, DuPont TA 2000), calibrated with indium, was used to monitor the changes of the thermal properties. All data were collected at a heating rate of 10 °C/min from −150 to 200 °C under N_2 atmosphere, after applying a heating cycle to remove water or other organic solvents: first run at a heating rate of 20 °C/min from 30 to 200 °C, following cooling step at a rate of 20 °C/min from 200 to −150 °C.

Results

Transformation in Crystal Structure and Morphology of Nanohybrids. A series of RAHs was prepared via an ionothermal process, where the concentration of [BMim][BF_4] was varied (see Experimental section on notation of RAHs). Figure 1 presents TEM and SEM images of RAH 2 and 4 as representatives of two 1D RAHs, respectively. RAH 2 (RAH 1−2) exhibited 1D nanorods with hexagonal tips, which were synthesized first,[4] obtaining a minimum diameter of ca. 25−50 nm, a maximum diameter of ca. 40−90 nm, and a length of ca. 1.3−1.6 μm. RAH 4 (RAH 3−5) displayed a 1D fibrous nanostructure with a length of ca. 40−60 nm and a diameter of ca. 1.5−3 nm. SAED patterns of the RAHs revealed diffused rings of fibrous RAHs, reflecting the existence of polycrystalline boehmite. Similarly, mixed patterns (ring and dot) of rodlike RAHs also revealed the presence of crystalline structures. The nanohybrids were not assembled into 1D nanoparticles below 20 wt % of [BMim][BF_4], whereas their sizes increased during a period of up to 2 days via the ionothermal process.

XRD patterns of RAH 1 and 2 were indexed to the hexagonal crystalline phase of aluminum hydroxide, whereas those of RAH 3 and 4 were assigned to typical orthorhombic boehmite phase, as given in Figure 2. Table 1 summarizes the chemical compositions, crystalline phases, and morphologies of the RAHs. In particular, two kinds of crystalline phases as well as respective morphologies were obtained with respect to the content of [BMim][BF_4]. The concentration of [BMim][BF_4] might affect the nucleation rate of aluminum precursors for the formation of nuclei, as the molecular structures of inorganic materials forming specific crystal phases can be kinetically tuned by various synthetic conditions such as temperature, pH, stoichiometry, the types of precursors, additives for rate control, templates, etc.[12] Taking into consideration that the intrinsic unit cell structure of the crystal phase is one of the critical parameters determining the shapes of inorganic crystalline materials,[5,13] the formation of a fibrous structure was associated with orthorhombic boehmite crystallites, whereas the construction of nanorods was related to hexagonal aluminum hydroxide crystallites.

The chemical structures of RAHs corresponding to respective crystalline phases were analyzed by ^{27}Al NMR spectra. Figure 3 presents ^{27}Al NMR spectra of RAHs, exhibiting three peaks at 5, 30, and 65 ppm from the coordinating species of aluminum-containing materials, assigned as six- (octahedral), five- (pentahedral), and four- (tetrahedral) coordinating sites.[14] Rod-shaped RAHs displayed large peaks from tetrahedral sites with small peaks from octahedral sites, whereas fibrous RAHs dominantly exhibited octahedral sites, simultaneously showing different chemical shifts from coordinating sites. In comparison to rod-shaped RAHs, fibrous RAHs had significantly more chemisorbed water above 100 °C, as shown in the TGA trace of Figure 4. Six-, five-, and four- coordinate species, which are created in the aluminum containing frameworks in order to preserve electron neutrality with OH ions of chemisorbed water, are determined by the intrinsic molecular structure of the crystal phase.[15,16] The differences in the relative ratio of the coordinating species of aluminum hydroxide, the location of peaks, and the content of chemisorbed water in the two RAHs were attributed to their distinct crystal phases, consisting of hydroxyl (Al−OH) centers and oxo (Al−O−Al) bridges, as well as to variation in the mutual interaction between cationic aluminums and chemisorbed water as a consequence of perturbation of hydrogen bonding by RTILs.[16] Therefore, the crystal phase, shape, and size of RAHs were determined by the concentration of [BMim][BF_4] and reaction time.

Solid−Liquid Phase Transition of Nanohybrids. The RAHs displayed various shapes and states with respect to the concen-

(11) Jung, Y. M.; Shin, H. S.; Czarnik-Matusewicz, B.; Noda, I.; Kim, S. B. *Appl. Spectrosc.* **2002**, *56*, 1568−1574.

(12) (a) Tang, B.; Ge, J.; Zhuo, L.; Wang, G.; Niu, J.; Shi, Z.; Dong, Y. *Eur. J. Inorg. Chem.* **2005**, 4366−4369. (b) Ahmadi, T. S.; Wang, Z. L.; Green, T. C.; Henglein, A.; El-Sayed, M. A. *Science* **1996**, *272*, 1924−1925. (c) Seo, W. S.; Shim, J. H.; Oh, S. J.; Lee, E. K.; Hur, N. H.; Park, J. T. *J. Am. Chem. Soc.* **2005**, *127*, 6188−6189.

(13) Yu, S. H.; Cölfen, H. *J. Mater. Chem.* **2004**, *14*, 2124−2147.

(14) (a) Pozarnsky, G. A.; McCormick, A. V. *J. Non-Cryst. Solid* **1995**, *190*, 212−225. (b) Bagshaw, S. A.; Pinnaviaia, T. J. *Angew. Chem., Int. Ed.* **1996**, *35*, 1102−1105.

(15) Bradley, S. M.; Hanna, J. V. *J. Am. Chem. Soc.* **1994**, 116, 7771−7783.

(16) (a) Fitzgerald, J. J.; Piedra, G.; Dec, S. F.; Seger, M.; Maciel, G. E. *J. Am. Chem. Soc.* **1997**, *119*, 783−7842. (b) Isobe, T.; Watanabe, T.; d'Espinose de la Caillerie, J. B.; Legrand, A. P.; Massiot, D. *J. Colloid Interface Sci.* **2003**, *261*, 320−324.

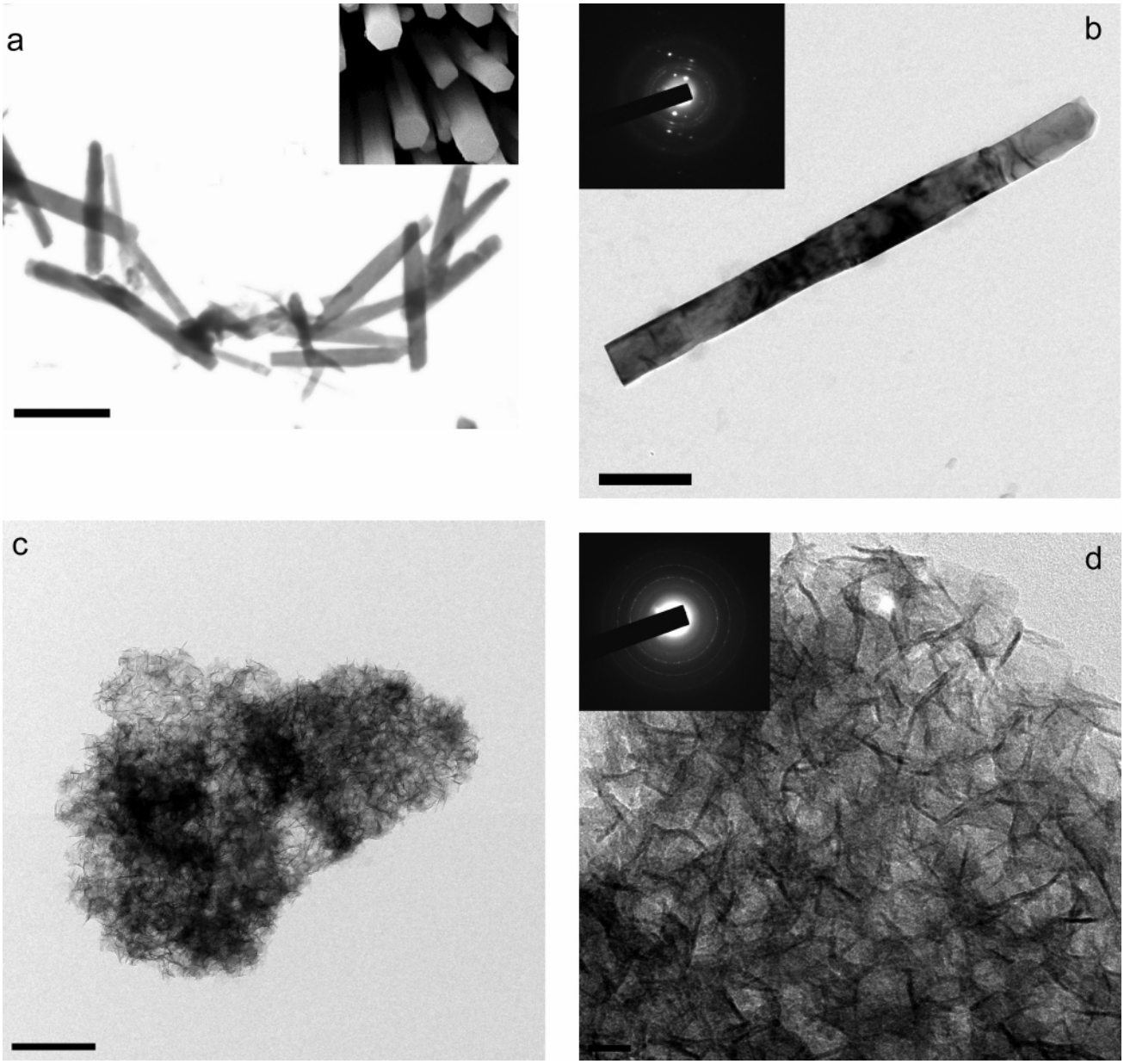

Figure 1. TEM images of (a) (1 μm bar, inset is SEM image) and (b) (200 nm bar, inset is SAED pattern) RAH 2 and (c) (200 nm bar) and (d) (20 nm bar, inset is SAED pattern) RAH 4.

tration of [BMim][BF_4], as shown in Figure 5. Rod-shaped RAHs showed a liquid-like state (RAH 1) or non-flowing transparent gel (RAH 2 as thin film) at high [BMim][BF_4] concentration, whereas fibrous RAHs displayed a nonmeltable white powder state (RAH 4 as powder) at low [BMim][BF_4] concentration. The states of RAHs indicate that the hierarchical transformation from orthorhombic (fibrous shaped nanosolid) to hexagonal structures (rodlike shaped nanoliquid) was strongly related with intermolecular interactions perturbed by the concentration of [BMim][BF_4]. Consequently, tuning of the material state played a crucial role in expanding the gallery of nanohybrids for applying nanopowder (boehmite crystallites, the boehmite phase of RAH 1 and 2, were transformed into $\gamma-$phase by calcinations above 400 °C) to a fixed bed in catalysis[3] and thin film (hexagonal crystallites) to a proton conductor in an electrochemical device.[4]

The confinement effect on the solid−liquid transition of RTILs and its relation to thermal properties should also be discussed, as [BMim][BF_4] (constituting cylindrical micelles) of RAHs was spatially confined inside cylindrical mesopores of aluminum hydroxides crystallites (constituting building blocks), as confirmed by the hysteresis loops of type IV H1 of the isolated aluminum hydroxides.[3,4] As seen in Figure 6, [BMim][BF_4] of one-pot assembled RAHs had high T_g compared to that of pristine [BMim][BF_4]. Taking into consideration the configurational entropy concept of Gibbs and DiMarzio, this is likely due to a reduction of the entropy as a consequence of spatial restriction of the fluid.[17] This hybrid system also exhibited a significant increase in T_m values with respect to the content of aluminum hydroxide, yielding broad endothermic peaks for hexagonal rodlike hybrids. In a similar trend to previous results,[18] T_g and T_m of the conventional hybrids

(17) (a) Gibbs, J. H.; DiMarzio, E. A. *J. Chem. Phys.* **1958**, *28*, 373−383. (b) DiMarzio, E. A.; Gibbs, J. H. *J. Chem. Phys.* **1958**, *28*, 807−813.
(18) Kanakubo, M.; Hiejima, Y.; Minami, K.; Aizawa, T.; Nanjo, H. *Chem. Commun.* **2006**, 1828−1830.

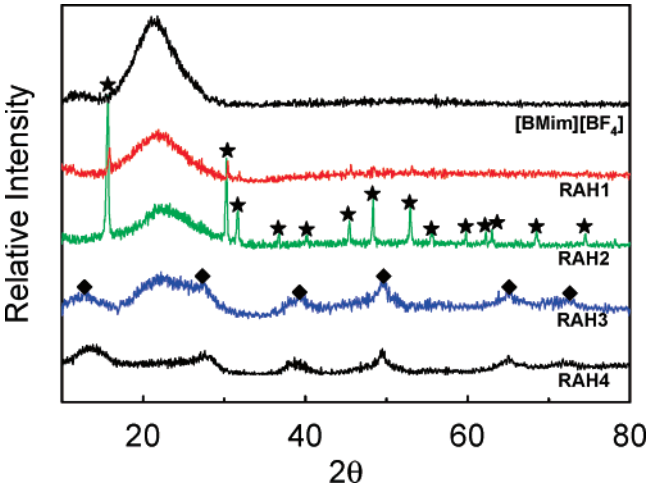

Figure 2. XRD patterns of [BMim][BF_4], RAH 1, RAH 2, RAH 3, and RAH 4. Asterisks were assigned to peaks of hexagonal crystalline aluminum hydroxide, whereas diamonds were assigned to those of orthorhombic boehmite phase.

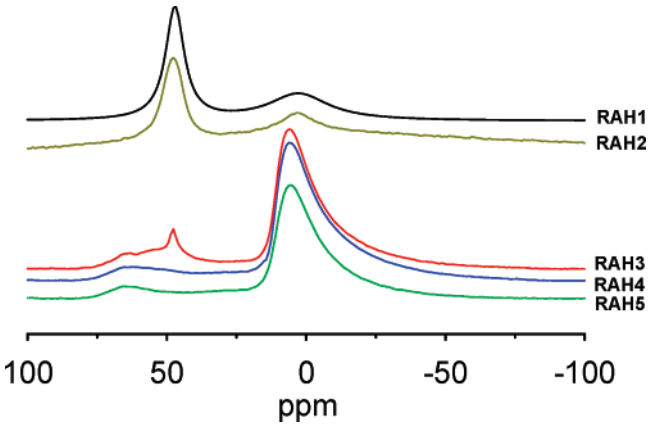

Figure 3. ^{27}Al NMR spectra of RAH 1, RAH 2, RAH 3, RAH 4, and RAH 5.

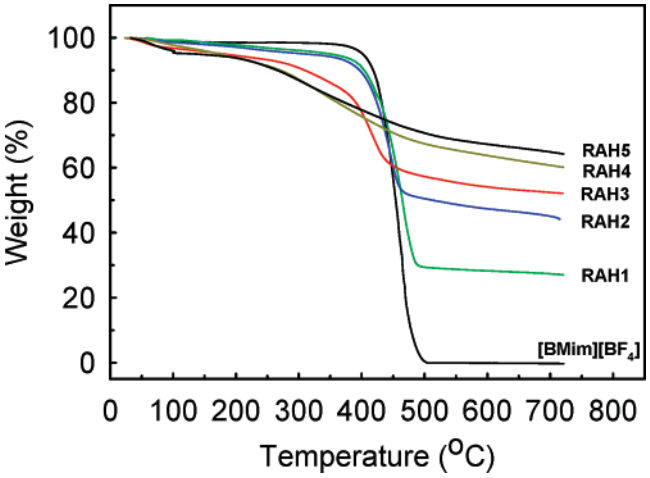

Figure 4. TGA curves of [BMim][BF_4], RAH 1, RAH 2, RAH 3, RAH 4, and RAH 5.

prepared by physical mixing of aluminum hydroxide with [BMim][BF_4] were reduced more steeply than those of bulk [BMim][BF_4], despite the almost identical textural property to the isolated RAH 2 (Table 2 and refer to inset of Figure 6 and Figure S1a and b for enlarged views of DSC curves). Wu et al. reported that [BMim][PF_6] possessed high melting points and

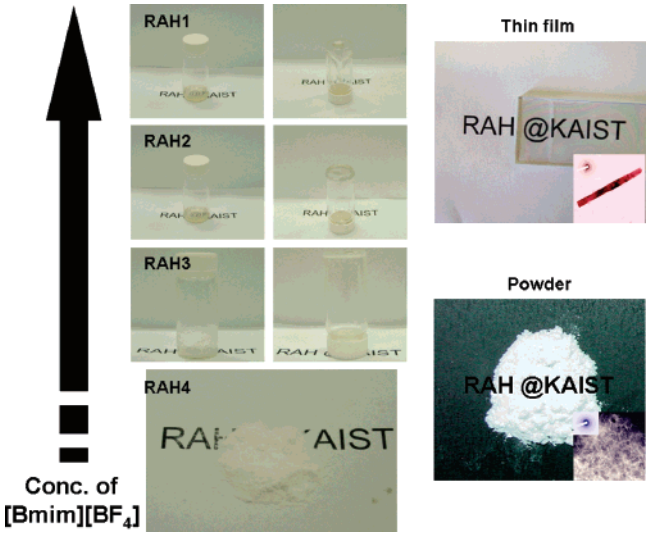

Figure 5. Photo images of RAH 1, 2, 3, and 4 (left side) and thin film of RAH 2 and powder of RAH 4 (right side).

showed ordering by means of secondary interactions when RTILs were encapsulated inside the thin channels of carbon nanotubes.[19] Similarly, the characteristic peak of imidazolium ring ordering at $2\theta = 19.980°$ appeared with an increase in the concentration of [BMim][BF_4], as shown in the XRD patterns. On the other hand, as the content of [BMim][BF_4] was decreased, the peaks corresponding to the respective crystal structures of aluminum hydroxide were dominant. This finding suggests that the RAHs exhibited reciprocal miscibility as a consequence of intermolecular interaction between [BMim][BF_4] and aluminum hydroxide crystallites.[20] Therefore, self-assembled [BMim][BF_4] inside RAHs also had higher T_g and T_m than those of pristine RTILs due to a confinement effect. Furthermore, considering the lower T_g and T_m of conventional hybrids, intermolecular interactions rather than the geometry of the restricted space in RAHs were the critical factor in enhancing transition temperatures. In addition to the enhancement of T_g and T_m, one-pot assembled nanohybrids showed a wide range of thermal decomposition, as shown in the TGA curves (Figure 4), indicating that intermolecular interactions between the fluid and the pore wall induced changes in the first or second phase transition behaviors of [BMim][BF_4] that are different from those of bulk and conventional hybrid materials arising from confinement effect.

Intermolecular Interaction-Induced Conformational Changes. To elucidate intermolecular interactions between RTILs and aluminum hydroxide crystallites, FT-IR and UV analyses were performed. Figure 7 shows FT-IR spectra of pristine [BMim][BF_4], RAH 1, RAH 2, RAH 3, and RAH 4. As the concentration of [BMim][BF_4] in RAHs was decreased, the characteristic peaks of BF_4^- anions and imidazolium rings at approximately 3000, 1570, 1460, 1170, and 1030 cm^{-1} were gradually weakened in the FT-IR spectra. In particular, two peaks above 3000 cm^{-1} in the IR spectra were regarded as diagnostic of changes in the CH···F hydrogen bonding between the BF_4^- anions and the 4,5-hydrogens of the imidazolium

(19) Chen, S.; Wu, G.; Sha, M.; Huang, S. *J. Am. Chem. Soc.* **2007**, *129*, 2416−2417.
(20) Yeon, S. H.; Kim, K. S.; Choi, S.; Cha, J. H.; Lee, H. *J. Phys. Chem. B* **2005**, *109*, 17928−17935.

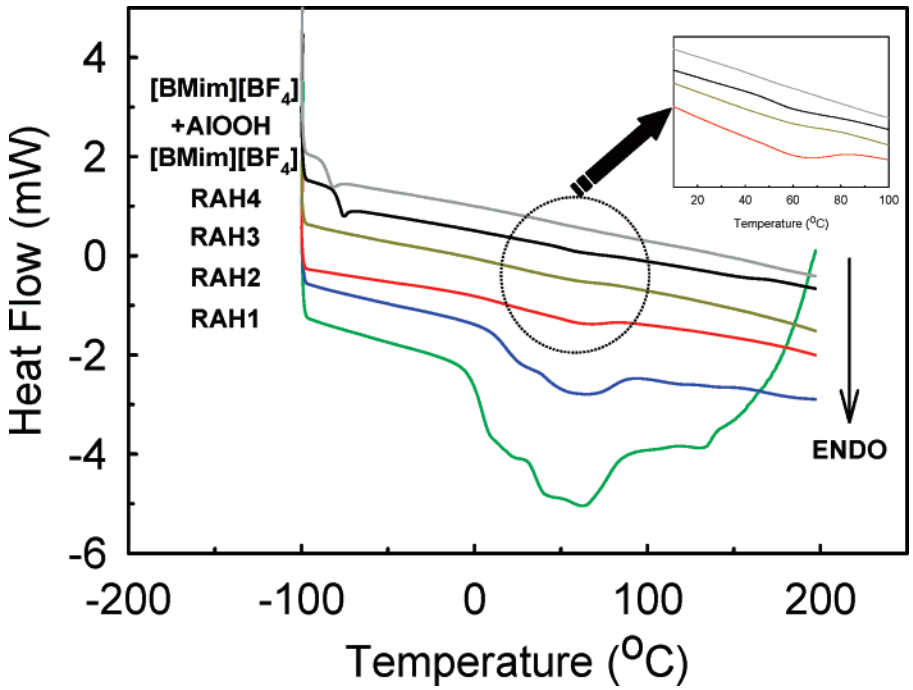

Figure 6. DSC curves of [BMim][BF_4]+AlOOH conventional mixture, [BMim][BF_4], RAH 1, RAH 2, RAH 3, and RAH 4. (Inset) Expanded view of [BMim][BF_4]+AlOOH conventional mixture, [BMim][BF_4], RAH 3, and RAH 4, marked with a circle.

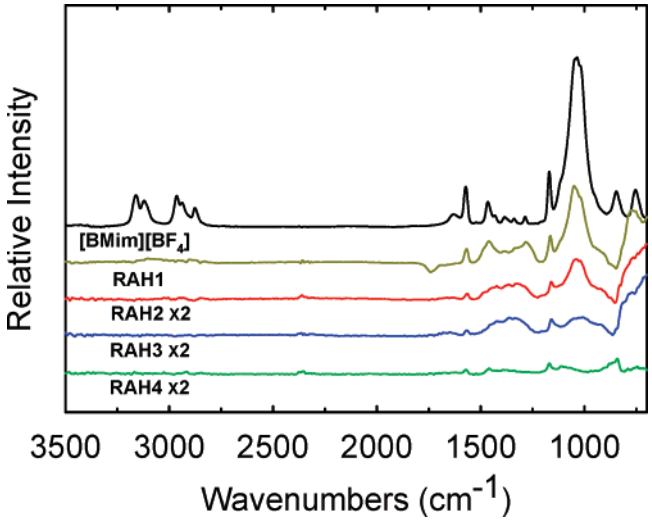

Figure 7. FT-IR spectra of [BMim][BF_4], RAH 1, RAH 2, RAH 3, and RAH 4.

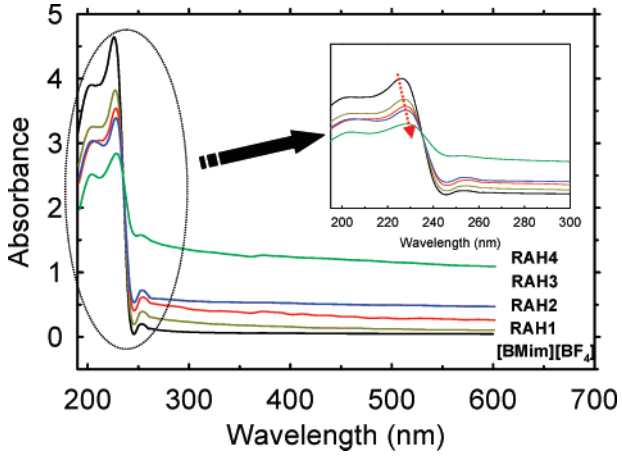

Figure 8. UV−vis spectra of [BMim][BF_4], RAH 1, RAH 2, RAH 3, and RAH 4. (Inset) Expanded view of spectra in a range of 200−300 nm.

ring.[21] In a RAH system, less electron density by means of polarization via hydrogen bonding led to a shift toward lower wavenumbers compared to the IR-spectra of pristine [BMim]-[BF_4].[3,22]

Figure 8 presents the UV spectra of pristine [BMim][BF_4], RAH 1, RAH 2, RAH 3, and RAH 4. In the UV spectra, the characteristic peak intensities of [BMim][BF_4] below 250 nm were decreased and showed a red-shift from 230 to 232 nm with respect to the content of aluminum hydroxides in RAHs (see inset of Figure 8). The variations in the peaks corresponding to BF_4^- anions and imidazolium rings of [BMim][BF_4] were consistent with the result that the self-assembly in the RTIL-induced shape formation (RISF) mechanism occurred via hydrogen bonding-co-$\pi-\pi$ stacking interactions; however, the spectra did not provide detailed information on conformational changes related to the interactions.

To clarify the intermolecular interactions as a function of the concentration of [BMim][BF_4], we applied 2D COS to the concentration-dependent FT-IR spectra. 2D COS is particularly suitable for elucidating physical interactions such as intra- and intermolecular interactions and complex self-assembled systems such as the RISF mechanism. Generated by a cross-correlation analysis of dynamic fluctuations of IR signals induced by an external perturbation such as temperature, time, stress, concentration, etc., 2D IR COS is defined by two independent wavenumbers.[10] In a synchronous 2D correlation spectrum, auto peaks located at the diagonal positions represent the overall susceptibility of the corresponding spectral region to change in

(21) Koel, M. *Proc. Estonian Acad. Sci. Chem.* **2000**, *49*, 145−155.
(22) Zhou, Y.; Schattka, J. H.; Antonietti, M. *Nano Lett.* **2004**, *4*, 477−481.
(23) (a) Cölfen, H.; Mann, S. *Angew. Chem., Int. Ed.* **2003**, *42*, 2350−2365. (b) Cölfen, H.; Antonietti, M. *Angew. Chem., Int. Ed.* **2005**, *44*, 5576−5591.

the spectral intensity as an external perturbation is applied to the system, whereas cross-peaks located at the off-diagonal positions of a synchronous 2D correlation spectrum reveal simultaneous or coincidental changes of spectral intensities observed at two different spectral variables (ν_1 and ν_2).[10] In contrast, an asynchronous 2D spectrum consisting of only cross-peaks provides useful information for interpreting the kinetics of chemical/physical interactions: the relative temporal relationship or order of the actual sequence of reorientation processes.[10]

Figure 9a shows a synchronous 2D correlation spectrum obtained from the concentration-dependent IR spectra of RAHs. Autopeaks, which appeared at around 1170 and 1030 cm^{-1}, are assigned to deformation vibration of the imidazolium ring and the stretching vibration of BF_4^-,[21] respectively. As shown in the top part of Figure 9a, the power spectrum extracted along a diagonal line in the synchronous spectrum demonstrates that the band at around 1030 cm^{-1} consisted of three bands at 1046, 1037, and 1020 cm^{-1} arising due to conformational change of BF_4^- anions. Furthermore, in the asynchronous 2D correlation spectrum (Figure 9b), the band for BF_4^- anions consisted of more bands at 1056, 1046, 1037, 1025, 1020, and 1012 cm^{-1}. A positive cross-peak at (1170, 1037) cm^{-1} in the synchronous 2D correlation spectrum indicates that the change of spectral intensity of the band at 1170 cm^{-1} was strongly interrelated with that at 1037 cm^{-1}. The apparently single peak at 1170 cm^{-1} was clearly resolved as two bands at 1173 and 1160 cm^{-1} in the asynchronous correlation spectrum. A 2D map, which plots the values of the first derivatives of the intensity with respect to concentration over the space of concentration vs wavenumber on a single map,[11] exhibited significant changes in the conformations of the imidazolium ring and BF_4^- anions via self-assembly during the formation of RAH 1 (Figure 9c). Three bands at 1160, 983, and 927 cm^{-1} were strongly sensitive to the phase transition from hexagonal to orthorhombic RAHs (from RAH 2 to RAH 3). In particular, the emergence of new peaks at 983 and 927 cm^{-1} was attributed to hierarchical transformations in the molecular structure, crystalline phase, and morphology of the RAHs. An analysis of the asynchronous 2D correlation spectrum reveals the following sequence of changes in spectral intensities: 1173 (conformational changed-peak of imidazolium ring) → 1037, 1025, 1020, and 1012 (conformational changed-peaks of BF_4^-) → 1056 and 1046 (conformational changed-peaks of BF_4^-) → 983 and 927 (peaks related to hierarchical transition) → 1160 cm^{-1} (peaks related to hierarchical transition). These results indicate that imidazolium rings and anions of the RTILs were reoriented spatially and conformational changes were carried out to compensate entropy changes during the self-assembly process. However, further studies involving computational simulations or correlation of conformational changes with X-ray data are required to verify the mechanism.

Discussion

In this work, a reciprocal transition of XRD and UV spectra occurred according to the relative content of [BMim][BF_4] and aluminum hydroxide crystallites (Figure 2 and Figure 2S). In particular, RAH 3 was observed in an intermediate state during this transition, where a rodlike gel with hexagonal crystal phase and a fibrous white powder with orthorhombic structure were mixed (Table 1 and Figure 3). Furthermore, micro- and macroscopic transformations in nanohybrids were accomplished

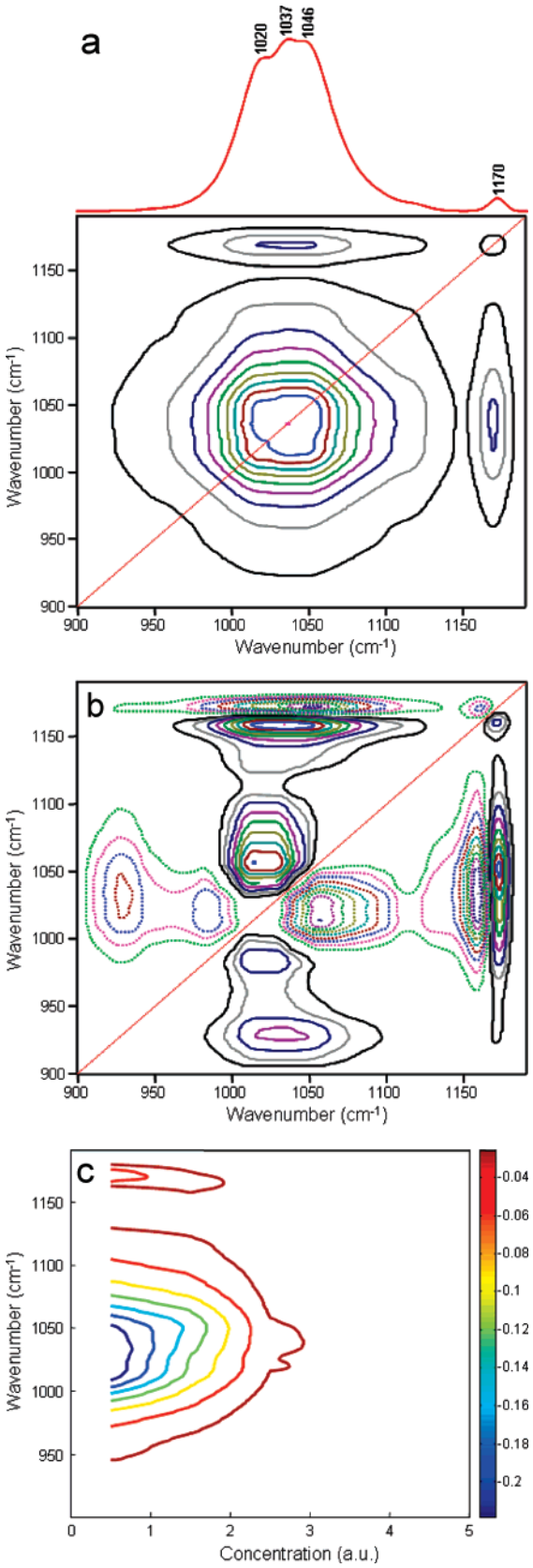

Figure 9. (a) Synchronous and (b) asynchronous 2D correlation spectra of RAHs as a function of concentration of [BMim][BF_4] in the range of 900−1190 cm^{-1}. Solid and dotted lines indicate regions of positive and negative correlation, respectively. (c) 2D map of the first derivatives of a set of spectra calculated with respect to concentration of [BMim][BF_4]. 0 was assigned to pristine [BMim][BF_4], 1 to RAH 1, 2 to RAH 2, 3 to RAH 3, 4 to RAH 4, and 5 to RAH 5.

under acidic conditions despite narrow pH variation (6.07 ± 0.11). These findings demonstrate that hierarchical transitions were relevant for the perturbation of intermolecular interactions by the concentration of [BMim][BF_4].

Diverse cooperative interactions between inorganic species and templates drive a variety of complex nanostructures and nanoshapes from inorganic or hybrid materials via organization and transformation.[23] In RTIL-templated systems, intermolecular interactions between RTILs (or template) and aluminum hydroxide crystallites (or building blocks) trigger the emergence of superstructures by influencing the force fields of secondary interactions, i.e., hydrogen bonding and $\pi-\pi$ stacking,[3,22] as verified by XRD, FT-IR, UV, and 2D IR COS. [BMim][BF_4] ionic liquid could strongly affect the formation of nuclei consisting of a specific crystal phase during the nucleation step due to its low interface energy and high directional polarizability in the reaction medium,[24] resulting in different crystal phases according to the concentration of [BMim][BF_4]. After the construction of building blocks with the respective crystal phases via nucleation and growth steps during the ionothermal process, the structures of nanohybrids were regulated by intermolecular interactions between RTILs and building blocks. Consequently, cooperative interactions via hydrogen bondings between BF_4^- anions of RTILs and hydroxyl groups of aluminum hydroxide crystallites and $\pi-\pi$ stacking of imidazolium rings, induced realignment of the building blocks along a specific direction with the minimization of surface energy. This was followed by transformation into specific structures of RTIL-inorganic nanohybrids through the oriented attachment of building blocks. The as-obtained 1D RAHs realized via an ionothermal process featured an integrated system wherein [BMim][BF_4] was spaciously confined within the porous walls of aluminum hydroxide crystallites. In RTIL-confined systems, intermolecular interactions between RTILs (or confined fluids) and aluminum hydroxide crystallites (or pore walls) rather than geometry played an important role of revealing solid−liquid transition, as confirmed by DSC results and textural properties. The conformational changes via self-assembly enable confined-[BMim][BF_4] to be reoriented inside the nanopores of the hybrids, thereby minimizing the surface energy. The melting temperatures of the confined-[BMim][BF_4] are then increased, compared to those of pristine and physical confined [BMim]-[BF_4]. Considering that the RTILs acted as fluids confined inside porous networks of an integrated hybrid system as well as template and cosolvent agents to form 1D nanostructures of nanohybrids via the ionothermal process, intermolecular interactions via hydrogen bonding and $\pi-\pi$ stacking comprised a dominant driving force for sequentially spatial reorientations and kinetically conformational changes invoking self-assembly and confinement effect of the nanohybrids, as monitored by 2D IR COS.

(24) Antonietti, M.; Kuang, D.; Smarsly, B.; Zhou, Y. *Angew. Chem., Int. Ed.* **2004**, *43*, 4988−4992.

Conclusion

We have demonstrated that intermolecular interactions between RTILs and inorganic materials led to the formation of two 1D shapes with respective crystal phases via self-assembly as well as unique thermal behaviors as a result of confinement effect. The nanohybrids were hierarchically transformed from orthorhombic to hexagonal structures, from fibrous to rodlike shapes, and from solid to liquid with respect to the concentration of RTILs. 2D COS analyses revealed that the hierarchical transformation involved conformational changes induced by intermolecular interactions between the RTIL and aluminum hydroxide crystallites through the following procedure: conformational changed-peak of imidazolium ring → conformational changed-peaks of BF_4^- → conformational changed-peaks of BF_4^- → peaks related to hierarchical transition → peaks related to hierarchical transition. These results indicate that tuning the molecular structures, morphologies, and phases of nanohybrids via hierarchical transformation is applicable to not only designing nanostructures of functional materials but also expanding the gallery of nanohybrids for application of nanopowders to fixed beds in catalysis and thin films to proton conductors in electrochemical devices.

Acknowledgment. We gratefully acknowledge the Genome-based Integrated Bioprocess Project of the Ministry of Science and Technology for financial assistance of these studies. We thank the Korea Basic Science Institute (KBSI) for the use of equipment for SEM, TEM, and ^{27}Al NMR measurements.

Supporting Information Available: Enlarged view of UV−vis spectra and changes in the absorbance at 230/300 nm as functions of the contents of [BMim][BF_4]/aluminum hydroxide in hybrids. This material is available free of charge via the Internet at http://pubs.acs.org.

JA073074K